Higher Order Time-Domain Finite-Element Method for Microwave Device Modeling With Generalized Hexahedral Elements

Nada J. Šekeljić, *Student Member, IEEE*, Milan M. Ilić, *Member, IEEE*, and Branislav M. Notaroš, *Senior Member, IEEE*

***Abstract*—A novel higher order and large-domain Galerkin-type finite-element method (FEM) is proposed for direct 3-D electromagnetic modeling in the time domain. The method is implemented in the time-domain finite-element method (TDFEM) analysis of multiport microwave waveguide devices with arbitrary metallic and dielectric discontinuities. It is based on the geometrical modeling using Lagrange-type interpolation generalized hexahedra of arbitrary geometrical-mapping orders, field expansion in terms of hierarchical curl-conforming 3-D polynomial vector basis functions of arbitrarily high field-approximation orders, time stepping with an implicit unconditionally stable finite-difference scheme invoking the Newmark-beta method, and mesh truncation introducing the waveguide port boundary condition. Numerical examples demonstrate excellent accuracy, efficiency, stability, convergence, and versatility of the presented method, and very effective large-domain TDFEM models of 3-D waveguide discontinuities using minimal numbers of large conformal finite elements and minimal numbers of unknowns. The results obtained by the higher order TDFEM are in an excellent agreement with indirect solutions obtained from the FEM analysis in the frequency domain (FD) in conjunction with the discrete Fourier transform and its inverse, as well as with measurements and with alternative full-wave numerical solutions in both time and FDs.**

***Index Terms*—Curved parametric elements, electromagnetic analysis, finite-element methods (FEMs), higher order modeling, microwave devices, numerical techniques, time-domain (TD) analysis, transient response, waveguide discontinuities.**

I. Introduction

THE finite-element method (FEM) has been effectively used in full-wave 3-D solutions to both open-region (e.g., antenna and scattering) and closed-region (e.g., waveguide and cavity) problems based on discretizing partial differential equations (PDEs) in electromagnetics [1]–[6]. The FEM has been well established as a method of choice for analysis and design of waveguide-based multiport passive microwave devices and systems, of arbitrary shapes and material compositions, in the frequency domain (FD) [7]–[11]. A rather disproportionate body of work exists, on the other hand, in the development of methods and tools for the FEM analysis and modeling in the time domain (TD) [1], [2], [6], [12]–[24] in spite of the fact that TD analysis and characterization of microwave structures and evaluation of associated transient electromagnetic phenomena are also of great practical importance for a number of well-established and emerging areas of microwave theory and engineering.

FEM techniques for direct modeling of electromagnetic phenomena in the TD (time-domain finite-element (TDFEM) techniques) are based on a direct numerical discretization of TD PDEs governing such phenomena (Maxwell's equations or wave equations in the TD) [1], [2], [6], [12]–[23]. Alternatively, the TD response of a microwave structure can be obtained indirectly, using the FEM analysis in the frequency domain [frequency-domain finite-element method (FDFEM)] in conjunction with the discrete Fourier transform (DFT) and the inverse discrete Fourier transform (IDFT) [24]. Efficient FDFEM-DFT/IDFT modeling of waveguide discontinuities and the first TD-from-FD FEM solver are presented in [24]. This present paper focuses on the TDFEM (direct) approach.

In terms of the particulars of the numerical discretization in space, practically all the existing 3-D TDFEM electromagnetic tools are low-order (also referred to as small-domain or sub-domain) techniques, with the electromagnetic structure being modeled by volume geometrical elements (most frequently, tetrahedra with planar sides) that are electrically very small and the fields within the elements are approximated by low-order (zeroth and first order) basis. This results in a very large number of unknowns (unknown field-distribution coefficients) needed to obtain results of satisfactory accuracy, with all the associated problems and large requirements in computational resources. An alternative approach, the higher order (also known as the large or entire domain) computational approach, which utilizes higher order basis functions defined in large curved geometrical elements, and which can greatly reduce the number of unknowns for a given problem and enhance the accuracy and efficiency of the computation [25], seems to have not been fully employed in the TDFEM analysis yet. Namely, almost none of the reported TDFEM results and applications in the literature demonstrate actual using and implementation of models of orders higher than two (high-order modeling). Notable examples

Manuscript received August 12, 2012; revised December 14, 2012; accepted December 19, 2012. Date of publication February 25, 2013; date of current version April 02, 2013. This work was supported by the National Science Foundation (NSF) under Grant ECCS-1002385 and by the Serbian Ministry of Education, Science and Technological Development under Grant TR-32005.

N. J. Šekeljić and B. M. Notaroš are with the Department of Electrical and Computer Engineering, Colorado State University, Fort Collins, CO 80523-1373 USA (e-mail: inadasek@engr.colostate.edu; notaros@colostate.edu).

M. M. Ilić is with the School of Electrical Engineering, University of Belgrade, 11120 Belgrade, Serbia, and also with the Department of Electrical and Computer Engineering, Colorado State University, Fort Collins, CO 80523-1373 USA (e-mail: milanilic@etf.rs).

Color versions of one or more of the figures in this paper are available online at http://ieeexplore.ieee.org.

Digital Object Identifier 10.1109/TMTT.2013.2246186

of high-order TDFEM modeling are the transfinite-element TD method for analysis of multiport waveguide structures proposed in [20], where nearly orthogonal Nedelec hierarchical bases of orders from 0 to 3 are used, and TDFEM solutions to cavity and waveguide problems in [23], where the results for hierarchical basis functions of up to mixed fourth order (order 3.5) on tetrahedral cells are presented. In addition, none of the works employ large elements (or a combination of large and small elements) in the TDFEM model (large-domain modeling).

This paper proposes a novel higher order and large-domain Galerkin-type FEM for 3-D electromagnetic modeling in the TD based on higher order geometrical modeling, higher order field modeling, and an implicit unconditionally stable time-stepping finite-difference scheme invoking the Newmark-beta method, and presents its implementation in the TDFEM analysis of multiport microwave waveguide devices with arbitrary metallic and dielectric discontinuities. The geometry of the structure is modeled using Lagrange-type interpolation generalized hexahedra of arbitrary geometrical-mapping orders, and the fields in the elements are expanded in terms of hierarchical curl-conforming 3-D polynomial vector basis functions of arbitrarily high field-approximation orders. The finite-element mesh is truncated introducing the waveguide port boundary condition (WPBC) at the waveguide ports, which is able to launch an incident wave into the waveguide and at the same time absorb the reflections from waveguide discontinuities in the 3-D TDFEM analysis [21]. Once the TD solution is obtained, the broadband frequency response (if needed) is computed applying the DFT to the TDFEM solution in the postprocessing.

To the best of our knowledge, this paper presents the first truly higher order 3-D TDFEM method (the results demonstrate using field expansions of orders from 2 to 9) and the first set of large-domain TDFEM modeling examples (the examples demonstrate very effective large-domain TDFEM models of 3-D waveguide discontinuities using minimal numbers of large conformal finite elements and minimal numbers of unknowns). Overall, the examples demonstrate excellent accuracy, efficiency, stability, convergence, and versatility of the presented method.

II. Formulation and Numerical Implementation

A. Finite-Element Spatial Discretization

Consider a general multiport waveguide structure with an arbitrary metallic and/or dielectric discontinuity shown in Fig. 1. In order to apply the FEM analysis, the computational domain is first truncated by imposing fictitious planar surfaces at each of the ports. The bounded structure thus obtained is then tessellated using Lagrange-type generalized parametric hexahedra of arbitrary geometrical orders K_u, K_v, and K_w $(K_u, K_v, K_w \geq 1)$, analytically described as [4]

$$\mathbf{r}(u,v,w) = \sum_{m=0}^{K_u}\sum_{n=0}^{K_v}\sum_{p=0}^{K_w} \mathbf{r}_{mnp}\, L_m^{K_u}(u)\, L_n^{K_v}(v)\, L_p^{K_w}(w) \qquad -1 \leq u,v,w \leq 1 \tag{1}$$

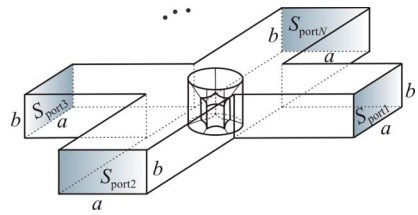

Fig. 1. 3-D multiport waveguide structure with an arbitrary discontinuity, simulated by a higher order TDFEM method.

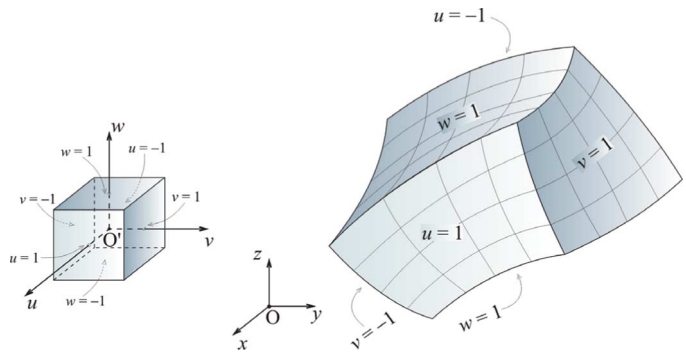

Fig. 2. Generalized curved parametric hexahedron defined by (1) and (2); cubical parent domain is also shown.

with $\mathbf{r}_{mnp} = \mathbf{r}(u_m, v_n, w_p)$ being the position vectors of interpolation nodes and $L_m^{K_u}$ representing Lagrange interpolation polynomials

$$L_m^{K_u}(u) = \prod_{l=0, l\neq m}^{K_u} \frac{u-u_l}{u_m-u_l} \tag{2}$$

and similarly for $L_n^{K_v}(v)$ and $L_p^{K_w}(w)$. Equations (1) and (2) define a mapping from a cubical parent domain to a generalized hexahedron, as shown in Fig. 2. The same Lagrange interpolating scheme is used to model continuously inhomogeneous material properties of a hexahedron (if applicable) in the mesh [11].

B. TDFEM Formulation

The general waveguide problem in Fig. 1 can be analyzed in the TD starting from the source-free time-dependent Maxwell's equations. Considering a linear, homogeneous or continuously inhomogeneous medium within a finite-sized computational domain V, bounded by the surface S, the following time-dependent electric field vector wave equation is obtained, which, together with associated initial and boundary conditions, defines a well-known boundary value problem [1], [6]

$$\nabla \times \frac{1}{\mu_r}\nabla \times \mathbf{E}(\mathbf{r},t) + \frac{1}{c_0^2}\varepsilon_r \frac{\partial^2 \mathbf{E}(\mathbf{r},t)}{\partial t^2} = 0 \tag{3}$$

where ε_r and μ_r are relative permittivity and permeability of the medium, respectively, and c_0 is the speed of light $(c_0 = 1/\sqrt{\varepsilon_0\mu_0})$. By multiplying (3) with space-dependant weighted (testing) vector functions (independent of time), $\mathbf{w}(\mathbf{r})$, integrating over the domain V (weighted residual method), and applying the first Green's vector identity, the

weak formulation of the vector wave equation in the TD is derived as follows:

$$\int_V \frac{1}{\mu_r}\left(\nabla\times\mathbf{w}\left(\mathbf{r}\right)\right)\cdot\left(\nabla\times\mathbf{E}\left(\mathbf{r},t\right)\right)dV + \oint_S \frac{1}{\mu_r}\left(\mathbf{n}\times\nabla\times\mathbf{E}\left(\mathbf{r},t\right)\right)\cdot\mathbf{w}\left(\mathbf{r}\right)dS + \frac{1}{c_0^2}\int_V \varepsilon_r\mathbf{w}\left(\mathbf{r}\right)\cdot\frac{\partial^2\mathbf{E}\left(\mathbf{r},t\right)}{\partial t^2}\,dV = 0 \tag{4}$$

with $\mathbf{n}$ standing for the outward-looking unit normal to the surface S. Within each finite element in Fig. 2, the time-variant electric field intensity vector is expanded using higher order hierarchical-type curl-conforming vector basis functions $\mathbf{f}$ and unknown time-dependent coefficients $\alpha(t)$

$$\begin{aligned}\mathbf{E}\left(\mathbf{r},t\right) = &\sum_{i=0}^{N_u-1}\sum_{j=0}^{N_v}\sum_{k=0}^{N_w}\alpha_{u\,i\,j\,k}(t)\,\mathbf{f}_{u\,i\,j\,k}\\ &+\sum_{i=0}^{N_u}\sum_{j=0}^{N_v-1}\sum_{k=0}^{N_w}\alpha_{v\,i\,j\,k}(t)\,\mathbf{f}_{v\,i\,j\,k}\\ &+\sum_{i=0}^{N_u}\sum_{j=0}^{N_v}\sum_{k=0}^{N_w-1}\alpha_{w\,i\,j\,k}(t)\,\mathbf{f}_{w\,i\,j\,k}\end{aligned} \tag{5}$$

where the functions $\mathbf{f}$ are defined as [4]

$$\begin{aligned}\mathbf{f}_{u\,i\,j\,k} &= u^i\,P_j\left(v\right)P_k\left(w\right)\mathbf{a}'_u\\ \mathbf{f}_{v\,i\,j\,k} &= P_i\left(u\right)v^j P_k\left(w\right)\mathbf{a}'_v\\ \mathbf{f}_{w\,i\,j\,k} &= P_i\left(u\right)P_j\left(v\right)w^k\,\mathbf{a}'_w.\end{aligned} \tag{6}$$

The P-functions are simple polynomials representing a higher order generalization of 1-D rooftop functions

$$P_i(u) = \begin{cases}1-u, & i=0\\ u+1, & i=1\\ u^i-1, & i\geq 2,\ \text{even}\\ u^i-u, & i\geq 3,\ \text{odd.}\end{cases} \qquad -1\leq u,v,w\leq 1 \tag{7}$$

Parameters N_u, N_v, and N_w ($N_u, N_v, N_w \geq 1$) are the adopted orders of the polynomials along the u-, v-, and w-directions of the local parametric coordinate system of each hexahedral element. Hierarchical functions $\mathbf{f}$ enable using different approximation orders in different elements in the model for efficient selective discretization of the solution domain because each lower order set of functions is a subset of higher order sets. The reciprocal unitary vectors $\mathbf{a}'_u$, $\mathbf{a}'_v$, and $\mathbf{a}'_w$ in (6) are obtained as $\mathbf{a}'_u = (\mathbf{a}_v\times\mathbf{a}_w)/J$, $\mathbf{a}'_v = (\mathbf{a}_w\times\mathbf{a}_u)/J$, and $\mathbf{a}'_w = (\mathbf{a}_u\times\mathbf{a}_v)/J$, with $J = (\mathbf{a}_u\times\mathbf{a}_v)\cdot\mathbf{a}_w$ being the Jacobian of the covariant transformation and $\mathbf{a}_u = \partial\mathbf{r}/\partial u$, $\mathbf{a}_v = \partial\mathbf{r}/\partial v$, and $\mathbf{a}_w = \partial\mathbf{r}/\partial w$ being the unitary vectors, where $\mathbf{r}$ is given in (1). Substituting (5) into (3) and applying the Galerkin testing procedure (testing functions are the same as basis functions), the following semidiscrete system of linear equations, expressed in the matrix form, is obtained:

$$[A]\left\{\alpha\left(t\right)\right\} + \frac{1}{c_0^2}[B]\frac{d^2\left\{\alpha\left(t\right)\right\}}{dt^2} = G \tag{8}$$

where the column vector of unknown coefficients is given by $\{\alpha(t)\} = \left\{\{\alpha_u(t)\},\{\alpha_v(t)\},\{\alpha_w(t)\}\right\}^T$, and the entries of matrices $[A]$ and $[B]$ are calculated as

$$\begin{aligned}A_{i,j} &= \int_V \frac{1}{\mu_r}\left(\nabla\times\mathbf{f}_i\right)\cdot\left(\nabla\times\mathbf{f}_j\right)dV\\ B_{i,j} &= \int_V \varepsilon_r\mathbf{f}_i\cdot\mathbf{f}_j\,dV, \qquad i=1,2,\ldots,N;\quad j=1,2,\ldots,N\end{aligned} \tag{9}$$

where $\mathbf{f}_i$ and $\mathbf{f}_j$ symbolically represent testing and basis functions defined in (6) and (7), and N is the total number of basis/testing functions. Note that matrices $[A]$ and $[B]$ are completely time-independent and are computed only once. The right-hand side of (8) is intentionally left in the form

$$G = -\oint_S \frac{1}{\mu_r}\mathbf{f}_i\cdot\left(\mathbf{n}\times\left(\nabla\times\mathbf{E}(\mathbf{r},t)\right)\right)dS \tag{10}$$

as this surface integral conveniently provides the interface for excitation and reflectionless truncation of the finite-element mesh, which is explained in Sections III and IV.

C. WPBC in the FD

Due to the continuity of the tangential component of the magnetic field intensity vector, $\mathbf{n}\times\mathbf{H}$, and hence, the vector $\mathbf{n}\times(\nabla\times\mathbf{E})$ in (10) across the interface between any two finite elements in the FEM model, the right-hand side in (8) contains the surface integral (10) across the overall boundary of the entire FEM domain, and not over the internal boundary surfaces between the individual finite elements in the model, which for the waveguide problem reduces to the surface integral across the waveguide ports. The total electric field vector at a cross section of a waveguide with discontinuities can be expressed as a superposition of the incident electric field and reflections from discontinuities that are modeled as a sum of orthogonal waveguide modes [1], [6]

$$\begin{aligned}&\mathbf{E}\left(x,y,z\right)\\ &\quad=\mathbf{E}^{\text{inc}}\left(x,y,z\right)\\ &\qquad+\sum_{m=0}^{\infty}\sum_{n=0}^{\infty}a_{m\,n}\mathbf{e}^{\text{TE}}_{t_{m\,n}}\left(x,y\right)e^{\gamma_{m\,n}z}+\\ &\qquad+\sum_{m=1}^{\infty}\sum_{n=1}^{\infty}b_{m\,n}[\mathbf{e}^{\text{TM}}_{t_{m\,n}}\left(x,y\right)+\hat{z}\mathbf{e}^{\text{TM}}_{z_{m\,n}}\left(x,y\right)]e^{\gamma_{m\,n}z}\end{aligned} \tag{11}$$

where $\mathbf{e}^{\text{TE}}_{t\,m\,n}$ and $\mathbf{e}^{\text{TM}}_{t\,m\,n}$ are transversal components of eigenfunctions for arbitrary TE and TM modes, respectively, and $\gamma_{m\,n}$ is the propagation constant of the corresponding mode. If the waveguide operates in the dominant-mode regime and it is assumed that the ports are placed far enough from all discontinuities, substituting (11) into $\mathbf{n}\times(\nabla\times\mathbf{E})$ in (10) and taking advantage of the orthogonality property of eigenfunctions, the following boundary condition at the ports can be derived:

$$\mathbf{n}\times\left(\nabla\times\mathbf{E}\right) = \begin{cases}-2\gamma_{10}\mathbf{E}^{\text{inc}}+\gamma_{10}\,\mathbf{E} & \text{(excitation port)}\\ \gamma_{10}\,\mathbf{E} & \text{(receiving ports)}\end{cases} \tag{12}$$

where, for a rectangular waveguide of transversal dimensions a and b ($a > b$), $\gamma_{10} = j\sqrt{k_0^2 - (\pi/a)^2}$, with $k_0 = 2\pi f/c_0$ being the free-space wavenumber and f being the operating frequency, $\mathbf{E}^{\rm inc} = E_0 \mathbf{e}_{10} e^{-\gamma_{10} z}$ at the excitation port, and $\mathbf{e}_{10} = \sqrt{2/(ab)} \sin(\pi x/a)\hat{\mathbf{y}}$.

D. WPBC in the TD

Since our goal is to analyze waveguide discontinuities directly in the TD, we employ the TD representation of the waveguide boundary condition in (12), as derived in [6] and [21], using the inverse Laplace transform (ILT) and applying it for the dominant mode. Before the ILT is applied to (12), γ_{10} can be expressed as follows:

$$\gamma_{10} = j\sqrt{k_0^2 - \left(\frac{\pi}{a}\right)^2} = \sqrt{\left(\frac{\pi}{a}\right)^2 - k_0^2} = \sqrt{\left(\frac{\pi}{a}\right)^2 + \left(\frac{s}{c_0}\right)^2}, \quad s = j\omega. \tag{13}$$

The ILT of the final equality in (13) can be found in [26] and it yields the following TD operator:

$$\Gamma_{10} = \frac{1}{c_0}\frac{d}{dt} + h_{10}(t) * \tag{14}$$

where $*$ stands for the convolution in the TD and $h_{10}(t)$ is the impulse response of the dominant waveguide mode, given by

$$h_{10}(t) = \frac{k_{10}}{t} J_1(k_{10} c_0 t)\, u(t) \tag{15}$$

with $k_{10} = \pi/a$, $u(t)$ denoting the unit step function, and J_1 denoting the first-kind Bessel function of the first order. Note that the singular point at $t = 0$ in (15) can be avoided by applying L'Hospital's rule and recurrence relation for derivative of the Bessel function $J_n'(z) = [J_{n-1}(z) - J_{n+1}(z)]/2$, where z is the argument of the Bessel function (in this case, $z = k_{10}c_0 t$). Therefore, at $t = 0$, the impulse response of the dominant waveguide mode is equal to $h_{10}(0) = k_{10}^2 c_0/2$. Now, combining expressions in (12), (14), (15), and (5), we can incorporate the TD boundary condition into the surface integral in (10) to obtain

$$\begin{aligned} G = &-\frac{1}{\mu_r}\left(\frac{1}{c_0}\frac{d}{dt} + h_{10}(t) *\right) \\ &\sum_{j=1}^{N} \alpha_j(t) \left[\oint_{S_1} (\mathbf{n}\times\mathbf{f}_i)\cdot(\mathbf{n}\times\mathbf{f}_j) dS + \oint_{S_2} (\mathbf{n}\times\mathbf{f}_i)\cdot(\mathbf{n}\times\mathbf{f}_j) dS\right] \\ &+ \frac{2}{\mu_r}\left(\frac{1}{c_0}\frac{d}{dt} + h_{10}(t) *\right) \oint_{S_1} \mathbf{f}_i \cdot \mathbf{E}^{\rm inc} dS, \\ &i = 1, 2, \ldots, N \end{aligned} \tag{16}$$

where S_1 and S_2 are the surfaces of the waveguide cross sections at the excitation and receiving ports, respectively. Due to the surface integration across the ports, only the unknown coefficients related to the tangential components of the vector basis functions at the ports are taken into account. Note that in (16), the TD operator Γ_{10} acts only on time-dependent unknown coefficients and the incident electric field. Substituting (16) into (8), we obtain the final semidiscretized spatial form of the vector wave equation

$$[A]\{\alpha(t)\} + \frac{1}{c_0^2}[B]\frac{d^2\{\alpha(t)\}}{dt^2} + \frac{1}{c_0\mu_r}[C]\frac{d\{\alpha(t)\}}{dt} + \frac{1}{\mu_r}[C]\{q_{10}(t)\} = \{f\} \tag{17}$$

where the entries of matrices $[C] = [C_1] + [C_2]$, $\{q_{10}(t)\}$, and $\{f\}$ are computed as

$$C_{p_{i,j}} = \oint_{S_p} (\mathbf{n}\times\mathbf{f}_i)\cdot(\mathbf{n}\times\mathbf{f}_j)\, dS, \quad p = 1, 2; \quad i, j = 1, 2, \ldots, N \tag{18}$$

$$\{q_{10}(t)\} = h_{10}(t) * \{\alpha(t)\} = \int_0^t h_{10}(t-\tau)\{\alpha(\tau)\}\, d\tau \tag{19}$$

$$\{f\} = \frac{2E_0}{\mu_r}\left[\frac{1}{c_0}\frac{d}{dt} f^{\rm inc}(t) + h_{10}(t) * f^{\rm inc}(t)\right] \oint_{S_1} (\mathbf{n}\times\mathbf{f}_i) \cdot (\mathbf{n}\times\mathbf{e}_{10})\, dS \tag{20}$$

and $f^{\rm inc}(t)$ stands for the incident pulse function.

E. Implicit Unconditionally Stable Time-Stepping Finite-Difference Scheme

Discretization of (17) in the TD can be done using different finite-difference schemes. The forward and backward difference approximations are first-order accurate, while the central difference approximation provides second-order accuracy. In addition, the forward-difference scheme is a numerically unstable method, the backward-difference scheme is unconditionally stable, and the central-difference scheme is a conditionally stable method, as shown in [1], [6], [13], and [14]. The most preferable and frequently used time-stepping scheme is the Newmark-beta method, which applies central differences for the first and second derivatives and a weighted average for the undifferentiated quantity [6]. It is shown in [27] that the Newmark-beta method is an implicit unconditionally stable scheme if $\beta \geq 1/4$ (β being the parameter that controls the accuracy and stability of the method). Employing this formulation for $\beta = 1/4$ to discretize (17) in the TD, we obtain

$$\frac{d^2\{\alpha(t)\}}{dt^2} = \frac{1}{\Delta t^2}\left[\{\alpha\}^{n+1} - 2\{\alpha\}^n + \{\alpha\}^{n-1}\right] \tag{21}$$

$$\frac{d\{\alpha(t)\}}{dt} = \frac{1}{2\Delta t}\left[\{\alpha\}^{n+1} - \{\alpha\}^{n-1}\right] \tag{22}$$

$$\{\alpha(t)\} = \frac{1}{4}\left[\{\alpha\}^{n+1} + 2\{\alpha\}^n + \{\alpha\}^{n-1}\right] \tag{23}$$

where the discrete-time representation of unknown field coefficients at a time step $t_n = n\Delta t$ is $\{\alpha(t)\} = \{\alpha(n\Delta t)\} = \{\alpha\}^n$. The initial state of the field inside the structure is defined

by the causality condition $\{\alpha(t)\} = \{0\}, t \leq 0$, and the convolution integral in (19) is discretized using the trapezoidal rule

$$\{q_{10}\}^n = \frac{\Delta t}{2}\left(h_{10}(0)\{\alpha\}^n + h_{10}(t_n)\{\alpha\}^0\right) + \Delta t \sum_{i=1}^{n-1} h_{10}((n-i)\Delta t)\{\alpha\}^i. \quad (24)$$

Finally, combining (21) –(24) yields the following unconditionally stable two-step update scheme:

$$[D_1]\{\alpha\}^{n+1} = \{f\}^n - [D_2]\{\alpha\}^{n-1} - [D_3]\{\alpha\}^n - \frac{1}{\mu_r}[C]\{q_{10}\}^n \quad (25)$$

with the $[D]$ matrices being given by

$$[D_1] = \frac{1}{4}[A] + \frac{1}{(c_0\Delta t)^2}[B] + \frac{1}{2\Delta t c_0 \mu_r}[C] \quad (26)$$

$$[D_2] = \frac{1}{4}[A] + \frac{1}{(c_0\Delta t)^2}[B] - \frac{1}{2\Delta t c_0 \mu_r}[C] \quad (27)$$

$$[D_3] = \frac{1}{2}[A] - \frac{2}{(c_0\Delta t)^2}[B]. \quad (28)$$

The resultant time-stepping scheme in (25) implies that the linear system of equations is solved at each time step, but the matrix $[D_1]$ on the left-hand side of the equation is inverted only once. Also, the discretized version of the impulse response in (15), as well as the convolution integral in (20), can be precalculated and stored in the memory before the marching in time starts. Unfortunately, the convolution on the left-hand side of (25) has to be computed at each time step, which significantly increases the overall simulation time. This problem can be remedied by a truncation of the impulse response in (15) or by performing the convolution in the form of a Toeplitz matrix–vector multiplication, as suggested in [21] and [28].

F. Modal Amplitudes at Waveguide Ports and Scattering Parameters

Once the matrix of unknown electric field coefficients $[\alpha]_{N\times N_t}$ is obtained solving (25), these coefficients are substituted back into (5), and the modal amplitudes of the dominant mode across the waveguide ports at each time step are calculated using the following expressions:

$$\begin{aligned} a_{10}(t) &= \int_{S_1} \mathbf{e_{10}} \cdot \left[\mathbf{E}(\mathbf{r},t) - \mathbf{E}^{\text{inc}}(\mathbf{r},t)\right]|_{z=z_1} dS \\ &= \int_{S_1} \mathbf{e_{10}} \cdot \mathbf{E}(\mathbf{r},t)\,|_{z=z_1}\, dS \\ &\quad - f^{\text{inc}}(t)\int_{S_1} \mathbf{e_{10}} \cdot \mathbf{e_{10}}|_{z=z_1}\, dS \text{ (at excitation port)} \\ b_{10}(t) &= \int_{S_2} \mathbf{e_{10}} \cdot \mathbf{E}(\mathbf{r},t)\,|_{z=z_2}\, dS \quad \text{(at receiving port)}. \end{aligned} \quad (29)$$

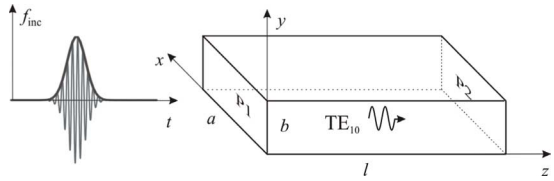

Fig. 3. Short empty rectangular waveguide section modeled by a single large finite-element (literally an entire-domain FEM model) and higher order TDFEM. Dimensions of the waveguide are $a = 10$ cm, $b = 5$ cm, and $l = 10$ cm.

Finally, the scattering parameters of the structure in Fig. 1 are computed as the ratio of the DFT of the modal amplitudes in (29), $A_{10}(f_k)$ and $B_{10}(f_k)$, respectively, to the DFT of the excitation pulse signal $F^{\text{inc}}(f_k)$

$$\begin{aligned} S_{11} &= \frac{\text{DFT}\{a_{10}(t_n)\}}{\text{DFT}\{f^{\text{inc}}(t_n)\}} = \frac{A_{10}(f_k)}{F^{\text{inc}}(f_k)} \\ S_{21} &= \frac{\text{DFT}\{b_{10}(t_n)\}}{\text{DFT}\{f^{\text{inc}}(t_n)\}} = \frac{B_{10}(f_k)}{F^{\text{inc}}(f_k)} \end{aligned} \quad (30)$$

where the DFT of a function in the TD can be computed as

$$\begin{aligned} F(f_k) = F(k) &= \sum_{n=0}^{N_f} f(t_n)\,\mathrm{e}^{-j(2\pi/N_f)\,nk} \\ f_k &= k\frac{f_s}{N_f}, \qquad k = 0,\ 1, \ldots, N_f - 1 \end{aligned} \quad (31)$$

with N_f standing for the number of frequency samples (in our case, $N_f = N_t$) and f_s for the sampling frequency.

III. Numerical Results and Discussion

As the first example, consider a short section of an empty rectangular waveguide, shown in Fig. 3. The waveguide section is modeled by means of a single FEM hexahedral element of the first geometrical order ($K_u = K_v = K_w = 1$), which, in this case, reduces to a brick. Note that this is literally an entire-domain FEM model (an entire computational domain is represented by a single finite element). In order to verify the numerical stability, accuracy, and convergence of the method, the waveguide is analyzed by the higher order TDFEM and the reflection coefficient, which theoretically vanishes, is computed in the frequency range from 1.5 to 4.5 GHz. (Note that $\lambda_g = 7.071$ cm at $f = 4.5$ GHz, λ_g being the wavelength of the TE_{10} mode.) Polynomial orders of the FEM field expansions are varied from $N_w = 2$ to $N_w = 9$ in the longitudinal waveguide direction, whereas they were kept constant, $N_u = 6$ and $N_v = 4$, along the longer and shorter waveguide cross-sectional sides, respectively. The waveguide is excited by a modulated Gaussian pulse given by

$$E_0(t) = \mathrm{e}^{-4\,(t-t_0/\sigma)^2}\sin\left[2\pi f_c\,(t-t_0)\right] \text{ V/m} \quad (32)$$

where the carrier frequency is $f_c = 3$ GHz, half-bandwidth is $\Delta f = 2.5$ GHz, $\sigma = 4/(\pi\Delta f)$, and $t_0 = 1.4\,\sigma$. The parameters of the time-marching process are: the total duration of the time signature $T = 10$ ns, the total number of time samples $N_t = 10\,000$, and the time step $\Delta t = T/(N_t - 1) \approx 1$ ps.

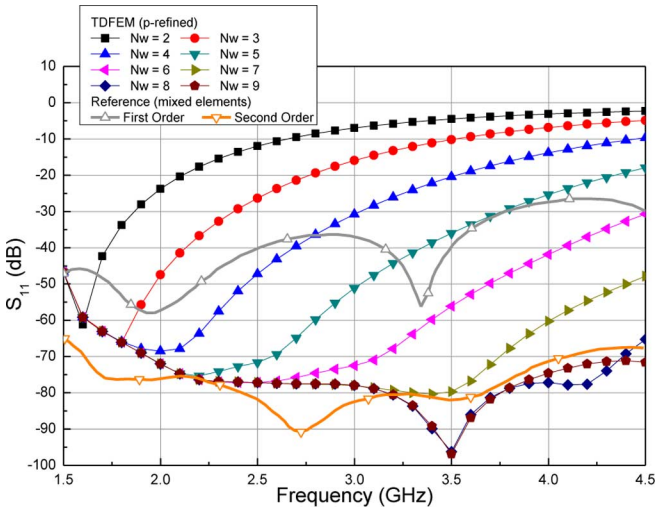

Fig. 4. Reflection coefficient for the TE_{10} mode in an empty rectangular waveguide in Fig. 3: convergence of the higher order TDFEM single-large-element results with p-refinement and comparison with the reference (h-refined mixed first- and second-order elements) results from [21].

The TD vector wave equation (already discretized in space applying the FEM) is solved at each time step using a direct solver, namely, Gaussian elimination. Note that iterative solvers [e.g., a conjugate gradient solver (CGS)] can also be used. In practical cases, the total simulation time or the total duration of the time signature, T, is determined as approximately twice the width of the input signal, which is usually a Gaussian or modulated Gaussian pulse, Neumann pulse (derivative of the Gaussian pulse), or a combination of Gaussian and Neumann pulses, or based on monitoring the reflections at the input port of the analyzed device [20]. Shown in Fig. 4 are the reflection coefficients versus frequency, computed using (30) from the TDFEM solution, for the p-refined single-large-element FEM model. The higher order TDFEM results are compared with the two results from [21], where a similar structure is analyzed, but the actual waveguide-section length and TD excitation parameters are not specified. The results show a stable behavior, as it is expected because of the Newmark-beta method, and excellent convergence properties with an extreme p-refinement. The reflection coefficient obtained by the higher order single-element TDFEM is on average practically equally low (around -75 dB in the given frequency span) as the one obtained by the mixed second order (h-refined) model from [21]. Note that the actual results will slightly vary with the choice of the excitation pulse and other parameters in the TD analysis (which are not explicitly given in [21]).

Shown in Table I are the computational requirements, in terms of the relative simulation time and memory, for analysis of the waveguide section in Fig. 3, for all p-refined solutions in Fig. 4, with the accuracy of individual solutions being given in Fig. 4. In TDFEM simulations, the time-marching process requires the maximum memory allocated at any point in time. During this process, the following matrices are allocated: $[D_1]$, $[D_2]$, $[D_3]$, and $[C]$, each of dimension $N \times N$, $[\alpha]$ and excitation matrix $[F]$, defined by (20), each of dimension $N \times N_t$, an $1 \times N_t$ array of impulse responses $\{h_{10}\}$, and two $1 \times N$ arrays, $\{q_{10}\}$ and $\{b\}$, where $\{b\}$ is a temporary array in

TABLE I
COMPUTATIONAL REQUIREMENTS FOR ANALYSIS OF THE WAVEGUIDE SECTION IN FIG. 3, FOR EIGHT p-REFINED SOLUTIONS

Expansion order, N_w	2	3	4	5	6	7	8	9
Number of unknowns, N	144	197	250	303	356	409	462	515
Relative simulation time	1	1.4	1.77	2.23	2.73	3.2	3.73	4.27
Memory (MB)	22.7	31.3	40.1	49.1	58.3	67.6	77.1	86.8

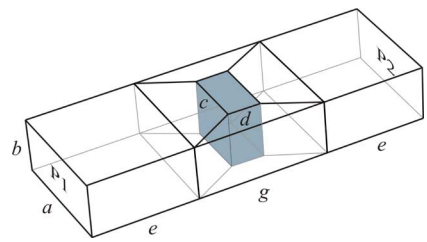

Fig. 5. WR-90 waveguide with a lossless dielectric ($\varepsilon_r = 8.2$) post and its large-domain hexahedral FEM mesh used in higher order TDFEM computations. Dimensions of the waveguide and mesh elements are $a = 22.86$ mm, $b = 10.16$ mm, $c = 12$ mm, $d = 6$ mm, $e = 45.72$ mm, and $g = 24$ mm.

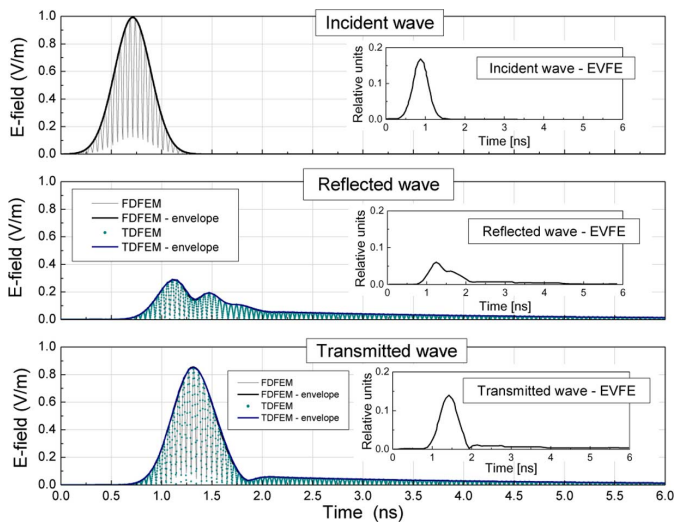

Fig. 6. Transient waveforms of incident, reflected, and transmitted waves for the structure in Fig. 5 and excitation in (32) obtained by the higher order TDFEM and FDFEM-DFT/IDFT [24] techniques (note that rectified modulated signals are shown within the envelopes); EVFE results from [29] are shown in the figure insets.

which the right-hand side of the TD [see (15), (24), and (25)] is stored during one pass through the time-marching loop. All computations are carried out without parallelization on an Intel Core 2 Quad CPU Q6600 at 2.4 GHz, with 8-GB RAM, under a 64-bit Windows 7 operating system.

The second example is an air-filled lossless WR-90 rectangular waveguide with a dielectric post, as shown in Fig. 5. The waveguide is operating in the single mode window; hence, the proper monomodal modeling is ensured by allowing a certain distance between the discontinuity and the waveguide ports, where the modal amplitudes of the electric field in (29) are computed by the higher order TDFEM. The waveguide is excited by the same type of modulated Gaussian pulse as in

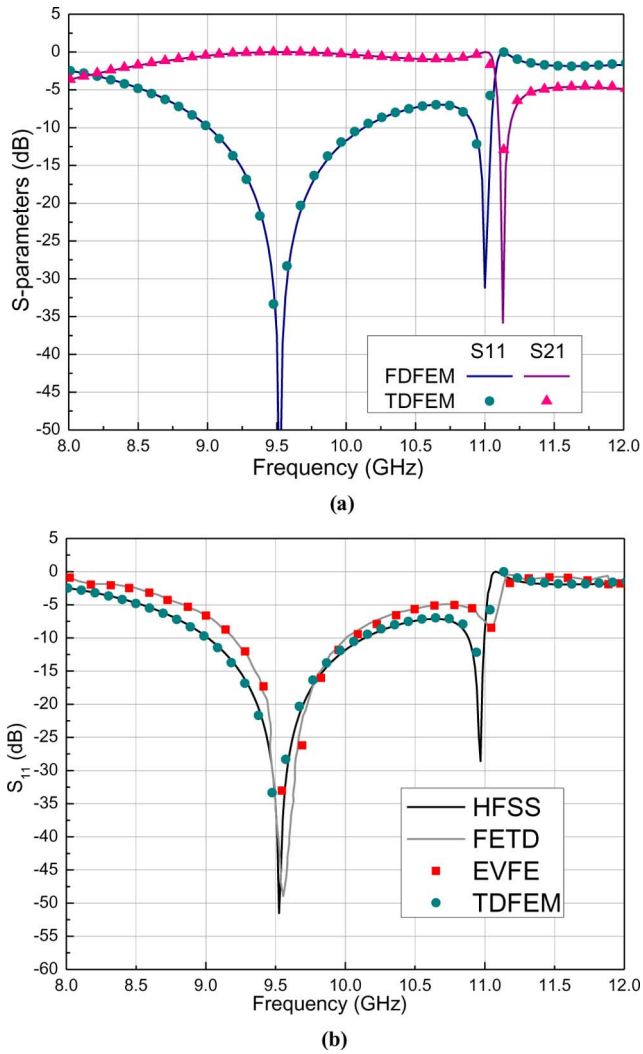

Fig. 7. Modal S-parameters of the waveguide structure in Fig. 5: comparison of higher order TDFEM results with: (a) FDFEM results [24] and (b) FETD [29], EVFE [29], and HFSS results.

(32) with $f_c = 10$ GHz, $\Delta f = 2.5$ GHz, $\sigma = 4/(\pi \Delta f)$, and $t_0 = 1.4\,\sigma$. The large-domain FEM mesh is constructed from only seven hexahedral elements (element dimensions vary from $0.2\lambda_g$ to $1.5327\lambda_g$ at $f = 12$ GHz) with $K_u = K_v = K_w = 1$ and N_u, N_v, and N_w ranging from 4 to 7 in different elements and different directions, which results in a total of 1791 FEM unknowns. The parameters of the time-marching process are $T = 10.235$ ns, $N_t = 5000$, and $\Delta t = 2.047$ ps. The obtained transient waveforms, shown in Fig. 6, are in an excellent agreement with FDFEM-DFT/IDFT results [24] and in a good agreement with envelope-finite-element (EVFE) responses from [29], bearing in mind that the results in [29] are obtained with a different waveguide excitation (current probes with no details provided), as opposed to modal excitations in this work, as well as that no details are provided in [29] about the actual locations of reference planes with respect to which the responses are given. Reflected and transmitted signals exhibit a stable behavior.

Next, we compute the S-parameters at the input and output ports in Fig. 5 [using (30)]. The sampling frequency is $f_s = 1/\Delta t = 488.52$ GHz (the number of DFT samples is equal

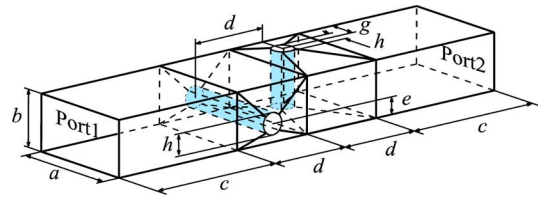

Fig. 8. Higher order large-domain hexahedral TDFEM model of a WR-62 waveguide with two crossed metallic cylindrical posts ($a = 15.7988$ mm, $b = 7.8994$ mm, $c = 20$ mm, $d = 11.51$ mm, $e = 2.5$ mm, $g = 4$ mm, $h = 3$ mm).

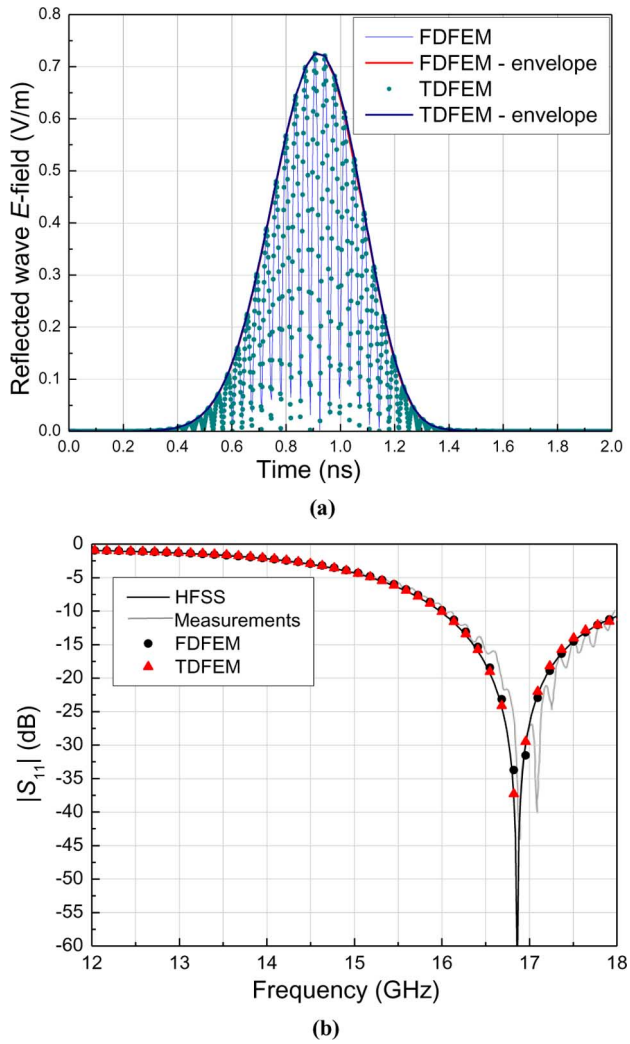

Fig. 9. Computed: (a) transient and (b) frequency responses for the waveguide structure in Fig. 8 using the higher order TDFEM: comparison with FDFEM-DFT/IDFT results [24] in (a) and with FDFEM results [24], HFSS results, and measurements [30] in (b).

to the number of samples in time, $N_f = N_t = 5000$). The higher order TDFEM results are shown in Fig. 7, where they are compared with FDFEM results [24] in Fig. 7(a) and with finite-element time-domain (FETD) (small-domain approximation, 72 373 tetrahedral elements, $\Delta x_{\min} = \Delta y_{\min} = \Delta z_{\min} = 1$ mm $\cong \lambda_g/30$, $\Delta t_{\max} = 1.9$ ps) [29], EVFE [29], and HFSS (commercial software, direct FD) results in Fig. 7(b). It can be concluded based on the figures that TDFEM results practically identically match FDFEM-DFT/IDFT results, as well as that

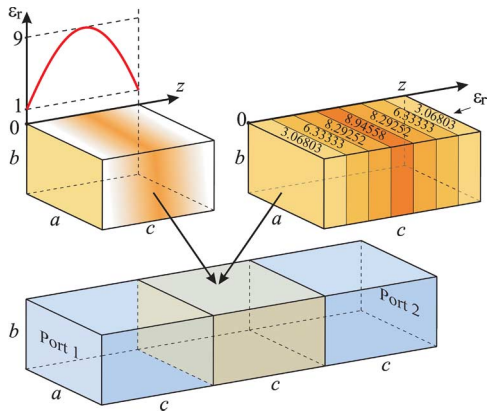

Fig. 10. Higher order large-domain TDFEM model of a WR-15 waveguide ($a = 3.76$ mm, $b = 1.88$ mm, and $c = 2.5$ mm) with a continuously inhomogeneous (quadratically varying) lossless dielectric load (central element); seven-layer approximate model of the load with piecewise constant approximation of the quadratic permittivity profile [24] is also shown.

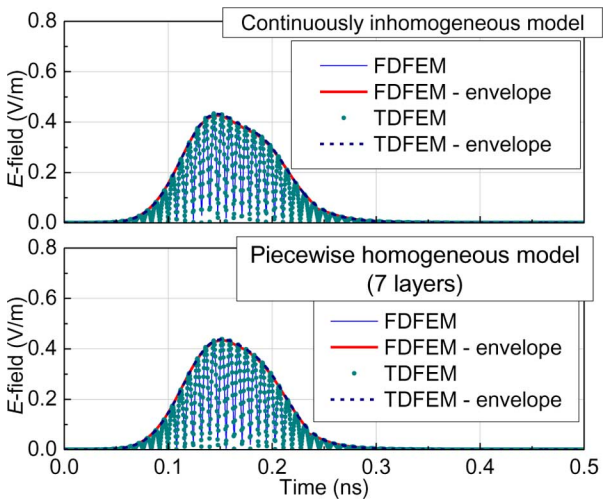

Fig. 11. Transient response for the reflected wave of the structure in Fig. 10: comparison of the higher order TDFEM and FEM-DFT/IDFT [24] results for the exact continuously inhomogeneous model and the approximate piecewise homogeneous model (with seven homogeneous layers), respectively (both models are shown in Fig. 10).

both sets of higher order results match the reference HFSS results extremely well, and in that sense, they both outperform the FETD and EVFE results.

As the third example, consider a WR-62 waveguide with two crossed metallic cylindrical posts, with the large-domain FEM model shown in Fig. 8 (ten generalized hexahedral elements, K_u, K_v, and K_w are 1 or 2, N_u, N_v, and N_w range from 2 to 5, yielding 1184 unknowns) and the excitation in the form of the signal in (32), where $f_c = 14$ GHz and $\Delta f = 3$ GHz. The transient and frequency responses of the structure computed by the higher order TDFEM ($\Delta t = 1.462$ ps and $N_t = 5000$) are shown in Fig. 9. In Fig. 9(a), we observe an excellent agreement between the TDFEM and FDFEM-DFT/IDFT [24] results for the reflected waveform. In Fig. 9(b), a very good agreement between the numerical results obtained by the TDFEM, FDFEM [24], and HFSS and the measured data [30] for the S_{11} of the structure is observed.

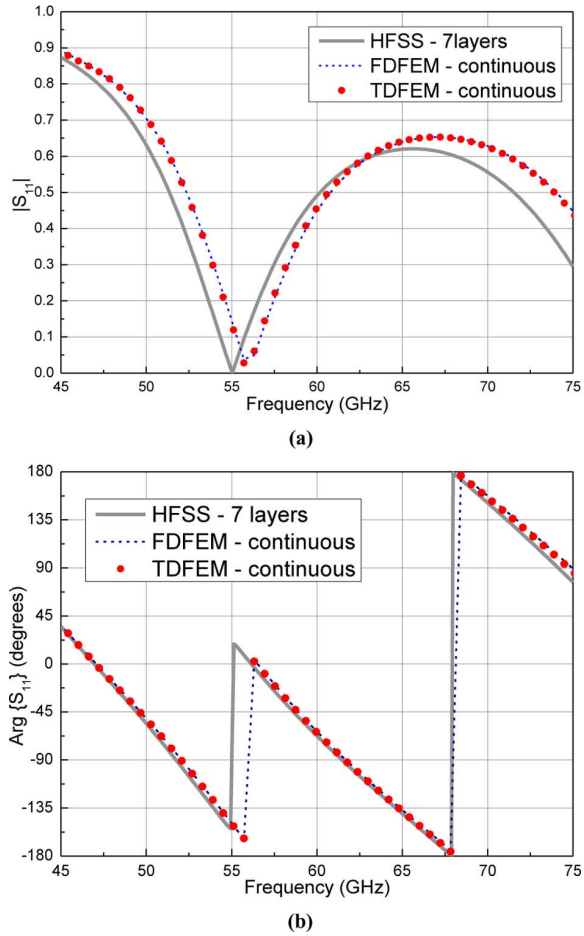

Fig. 12. (a) Magnitude and (b) phase (argument) of the S_{11}-parameter of the waveguide structure in Fig. 10 obtained by the higher order TDFEM and FDFEM [24], respectively, applied to the exact continuously inhomogeneous model and by HFSS applied to the approximate seven-layer model.

As the last example, we consider a WR-15 waveguide loaded with a continuously inhomogeneous dielectric slab with a relative permittivity profile given by $\varepsilon_r(u) = 9 - 8u^2$, $-1 < u < 1$, and $u = 2z/c - 1$, as depicted in Fig. 10. The transient responses for the reflected wave obtained by the higher order TDFEM (excitation in (32), $f_c = 62$ GHz, $\Delta f = 15$ GHz, $\Delta t = 0.33$ ps, and $N_t = 5000$) for: (A) an exact continuously inhomogeneous model and (B) an approximate piecewise homogeneous model are shown in Fig. 11. Model (A), with the entire slab represented by a single continuously inhomogeneous finite element, consists of only three hexahedral finite elements with $K_u = K_v = K_w = 1$ (one inhomogeneous dielectric element with $N_u = 4$, $N_v = 2$, and $N_w = 7$ and two buffer elements with $N_u = 4$, $N_v = 2$, and $N_w = 4$) and requires only 205 unknowns. Model (B), with the slab approximated by seven homogeneous layers (relative permittivities of layers are given in Fig. 10), includes nine hexahedral elements ($K_u = K_v = K_w = 1$, N_u, N_v, and N_w range from 2 to 5) and results in 569 unknowns [24]. The results of the FEM-DFT/IDFT simulations for both models [24] are included for comparison. It can be observed from the figure that, in both cases, the TDFEM and FEM-DFT/IDFT results are practically identical, as well as that the transient responses for the continuously inhomogeneous model and the seven-layer model agree very well. Note

that for model (A), the TDFEM simulation takes 2.5 times less computational time than the FEM-DFT/IDFT simulation, while the TDFEM simulation of model (B) takes 34% more computational time than the FEM-DFT/IDFT simulation. Note also that the FEM-DFT/IDFT solver takes advantage of an extremely fast multifrequency FDFEM analysis of 3-D waveguide structures (the global FEM matrix is filled only once and then reused for every subsequent frequency point) needed for the inverse Fourier transform [24].

The computed S_{11}-parameter of the structure in Fig. 10 is shown in Fig. 12. In the graphs, the TDFEM solution with the continuously inhomogeneous model is compared with the FDFEM solution for the same model and with the HFSS solution for the seven-layer model. We observe an excellent agreement of the TDFEM and FDFEM-DFT/IDFT results and a very good agreement of both sets of higher order results with the HFSS solution (TDFEM and FDFEM-DFT/IDFT solutions for the seven-layer model, being in excellent agreement with the HFSS results, are not shown).

IV. Conclusions

This paper has proposed a novel higher order and large-domain Galerkin-type FEM for direct 3-D electromagnetic modeling in the TD and has presented its implementation in the TDFEM analysis of multiport microwave waveguide devices with arbitrary metallic and dielectric discontinuities. The method is based on the geometrical modeling using Lagrange-type interpolation generalized hexahedra of arbitrary geometrical-mapping orders, field expansion in terms of hierarchical curl-conforming 3-D polynomial vector basis functions of arbitrarily high field-approximation orders, time-stepping with an implicit unconditionally stable finite-difference scheme invoking the Newmark-beta method, and mesh truncation introducing the WPBC.

Numerical examples of waveguide structures that include metallic and homogeneous and continuously inhomogeneous dielectric discontinuities have validated the method, which appears to be the first truly higher order 3-D TDFEM technique (the results have demonstrated using field expansions of orders from 2 to 9), and have demonstrated its excellent accuracy, efficiency, stability, convergence, and versatility. They have demonstrated very effective large-domain TDFEM models of 3-D waveguide discontinuities using minimal numbers (from one to ten) of large conformal finite elements and minimal numbers (up to 1791) of unknowns, which appear to be the first set of large-domain TDFEM modeling examples. The results obtained by the higher order TDFEM are in excellent agreement with the FDFEM-DFT/IDFT solutions, as well as with measurements and with alternative full-wave numerical solutions in both the TD and FD.

References

[1] J. M. Jin, *The Finite Element Method in Electromagnetics*, 2nd ed. New York, NY, USA: Wiley, 2002.

[2] P. P. Silvester and R. L. Ferrari, *Finite Elements for Electrical Engineers*, 3rd ed. Cambridge, U.K.: Cambridge Univ. Press, 1996.

[3] J. L. Volakis, A. Chatterjee, and L. C. Kempel, *Finite Element Method for Electromagnetics*. New York, NY, USA: IEEE Press, 1998.

[4] M. M. Ilić and B. M. Notaroš, "Higher order hierarchical curved hexahedral vector finite elements for electromagnetic modeling," *IEEE Trans. Microw. Theory Techn.*, vol. 51, no. 3, pp. 1026–1033, Mar. 2003.

[5] M. M. Ilić, M. Djordjević, and B. M. Notaroš, "Higher order hybrid FEM-MoM technique for analysis of antennas and scatterers," *IEEE Trans. Antennas Propag.*, vol. 57, no. 5, pp. 1452–1460, May 2009.

[6] J. M. Jin and D. J. Rieley, *Finite Element Analysis of Antennas and Arrays*. New York, NY, USA: Wiley, 2009.

[7] J. Rubio, J. Arroyo, and J. Zapata, "Analysis of passive microwave circuits by using a hybrid 2-D and 3-D finite-element mode-matching method," *IEEE Trans. Microw. Theory Techn.*, vol. 47, no. 9, pp. 1746–1749, Sep. 1999.

[8] J. Liu, J. M. Jin, E. K. N. Yung, and R. S. Chen, "A fast, higher order three-dimensional finite-element analysis of microwave waveguide devices," *Microw. Opt. Technol. Lett.*, vol. 32, no. 5, pp. 344–352, Mar. 2002.

[9] E. Martini, G. Pelosi, and S. Selleri, "A hybrid finite-element–modal-expansion method with a new type of curvilinear mapping for the analysis of microwave passive devices," *IEEE Trans. Microw. Theory Techn.*, vol. 51, no. 6, pp. 1712–1717, Jun. 2003.

[10] M. M. Ilić, A. Ž. Ilić, and B. M. Notaroš, "Higher order large-domain FEM modeling of 3-D multiport waveguide structures with arbitrary discontinuities," *IEEE Trans. Microw. Theory Techn.*, vol. 52, no. 6, pp. 1608–1614, Jun. 2004.

[11] M. M. Ilić, A. Ž. Ilić, and B. M. Notaroš, "Continuously inhomogeneous higher order finite elements for 3-D electromagnetic analysis," *IEEE Trans. Antennas Propag.*, vol. 57, no. 9, pp. 2798–2803, Sep. 2009.

[12] A. C. Cangellaris, C. C. Lin, and K. K. Mei, "Point-matched time-domain finite element methods for electromagnetic radiation and scattering," *IEEE Trans. Antennas Propag.*, vol. AP-35, no. 10, pp. 1160–1173, Oct. 1987.

[13] J. F. Lee, "WETD—A finite element time-domain approach for solving Maxwell's equations," *IEEE Microw. Guided Wave Lett.*, vol. 4, no. 1, pp. 11–13, Jan. 1994.

[14] J. F. Lee, R. Lee, and A. C. Cangellaris, "Time-domain finite element methods," *IEEE Trans. Antennas Propag.*, vol. 45, no. 3, pp. 430–442, Mar. 1997.

[15] M. R. Zunoubi, K. C. Donepudi, J. M. Jin, and W. C. Chew, "Efficient time-domain and frequency-domain finite-element solution of Maxwell's equations using spectral Lanczos decomposition method," *IEEE Trans. Microw. Theory Techn.*, vol. 46, no. 8, pp. 1141–1149, Aug. 1998.

[16] D. Jiao and J. M. Jin, "Time-domain finite-element modeling of dispersive media," *IEEE Microw. Wireless Compon. Lett.*, vol. 11, no. 5, pp. 220–222, May 2001.

[17] D. Jiao and J. M. Jin, "Time-domain finite-element simulation of cavity-backed microstrip patch antenna," *Microw. Opt. Technol. Lett.*, vol. 32, no. 4, pp. 251–254, Feb. 2002.

[18] D. Jiao, A. A. Ergin, B. Shanker, E. Michielssen, and J. M. Jin, "A fast higher-order time-domain finite element-boundary integral method for 3-D electromagnetic scattering analysis," *IEEE Trans. Antennas Propag.*, vol. 50, no. 9, pp. 1192–1202, Sep. 2002.

[19] D. Jiao and J. M. Jin, "Three-dimensional orthogonal vector basis functions for time-domain finite-element solution of vector wave equations," *IEEE Trans. Antennas Propag.*, vol. 51, no. 1, pp. 59–66, Jan. 2003.

[20] D. K. Sun, J. F. Lee, and Z. Cendes, "Transfinite-element time-domain method," *IEEE Trans. Microw. Theory Techn.*, vol. 51, no. 10, pp. 2097–2105, Oct. 2003.

[21] Z. Lou and J. M. Jin, "An accurate waveguide port boundary condition for the time-domain finite-element method," *IEEE Trans. Microw. Theory Techn.*, vol. 53, no. 9, pp. 3014–3023, Sep. 2005.

[22] J. M. Jin, Z. Lou, Y. J. Li, N. W. Riely, and D. J. Riely, "Finite element analysis of complex antennas and arrays," *IEEE Trans. Antennas Propag. (Special Issue)*, vol. 56, no. 8, pt. I, pp. 2222–2240, Aug. 2008.

[23] N. Marais and D. B. Davidson, "Numerical evaluation of high-order finite element time domain formulations in electromagnetics," *IEEE Trans. Antennas Propag.*, vol. 56, no. 12, pp. 3743–3751, Dec. 2008.

[24] E. M. Klopf, S. B. Manić, M. M. Ilić, and B. M. Notaroš, "Efficient time-domain analysis of waveguide discontinuities using higher order FEM in frequency domain," *Progr. Electromagn. Res.*, vol. 120, pp. 215–234, 2011.

[25] B. M. Notaroš, "Higher order frequency-domain computational electromagnetics," *IEEE Trans. Antennas Propag. (Special Issue)*, vol. 56, no. 8, pp. 2251–2276, Aug. 2008.

[26] M. Abramowitz and I. Stegun, *Handbook of Mathematical Functions*. New York, NY, USA: Dover, 1970.
[27] S. D. Gedney and U. Navsariwala, "An unconditionally stable finite element time-domain solution of the vector wave equation," *IEEE Microw. Guided Wave Lett.*, vol. 5, no. 10, pp. 332–334, Oct. 1995.
[28] A. E. Yilmaz, D. S. Weile, B. Shanker, J. M. Jin, and E. Michielssen, "Fast analysis of transient scattering in lossy media," *IEEE Antennas Wireless Propag. Lett.*, vol. 1, no. 1, pp. 14–17, Dec. 2002.
[29] H. P. Tsai, Y. Wang, and T. Itoh, "Efficient analysis of microwave passive structures using 3-D envelope-finite element (EVFE)," *IEEE Trans. Microw. Theory Techn.*, vol. 50, no. 12, pp. 2721–2727, Dec. 2002.
[30] R. Bunger and F. Arndt, "Moment-method analysis of arbitrary 3-D metallic N-port waveguide structures," *IEEE Trans. Microw. Theory Techn.*, vol. 48, no. 4, pp. 531–537, Apr. 2000.

Nada J. Šekeljić (S'11) was born in Belgrade, Serbia, in 1984. She received the Dipl. Ing. (B.Sc.) degree in electrical engineering from the University of Belgrade, Belgrade, Serbia, in 2008, and is currently working toward the Ph.D. degree at Colorado State University, Fort Collins, CO.

Since 2008, she has been a Research Assistant with the Electromagnetics Laboratory, and Teaching Assistant with the Department of Electrical and Computer Engineering, Colorado State University. Her research interests are computational and applied electromagnetics.

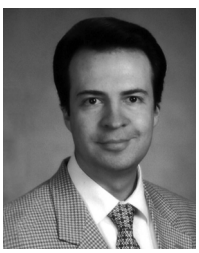

Milan M. Ilić (S'00–M'04) was born in Belgrade, Serbia, in 1970. He received the Dipl. Ing. and M.S. degrees in electrical engineering from the University of Belgrade, Belgrade, Serbia, in 1995 and 2000, respectively, and the Ph.D. degree from the University of Massachusetts Dartmouth, Dartmouth, MA, USA, in 2003.

He is currently an Associate Professor with the School of Electrical Engineering, University of Belgrade, and a Postdoctoral Research Associate and Affiliated Faculty Member with the Electrical and Computer Engineering Department, Colorado State University. His research interests include computational electromagnetics, antennas, and microwave components and circuits.

Dr. Ilić served as Technical Program Committee chair for the 11th International Workshop on Finite Elements for Microwave Engineering (FEM2012), June 4–6, 2012, Estes Park, CO, USA. He was the recipient of the 2005 IEEE Microwave Theory and Techniques Society (IEEE MTT-S) Microwave Prize.

Branislav M. Notaroš (M'00–SM'03) was born in Zrenjanin, Yugoslavia, in 1965. He received the Dipl. Ing. (B.S.), M.S., and Ph.D. degrees in electrical engineering from the University of Belgrade, Belgrade, Serbia, in 1988, 1992, and 1995, respectively.

From 1996 to 1999, he was an Assistant Professor with the School of Electrical Engineering, University of Belgrade. From 1998 to 1999, he spent the academic year as a Visiting Scholar with the University of Colorado at Boulder. From 1999 to 2004, he was an Assistant Professor, and from 2004 to 2006, an Associate Professor with the Department of Electrical and Computer Engineering, University of Massachusetts Dartmouth. From 2006 to 2012, he was an Associate Professor with the Department of Electrical and Computer Engineering, Colorado State University, Fort Collins, CO, USA. He is currently a Professor and Director of the Electromagnetics Laboratory, Colorado State University. His publications include over 100 journal and conference papers and three workbooks in electromagnetics and in fundamentals of electrical engineering (basic circuits and fields). He authored the textbook *Electromagnetics* (Prentice-Hall, 2010) for undergraduates, as well the the Electromagnetics Concept Inventory (EMCI), an assessment tool for electromagnetic fields and waves. His research interests and activities are computational electromagnetics, antennas, scattering, microwaves, and metamaterials, and in particular, higher order computational electromagnetic techniques based on the method of moments, FEM, physical optics, domain decomposition method, diakoptics, and hybrid methods as applied to modeling and design of antennas, scatterers, and microwave and optical devices.

Dr. Notaroš was general chair for the 11th International Workshop on Finite Elements for Microwave Engineering (FEM2012), Estes Park, CO, USA, June 4–6, 2012. He was the recipient of the 2005 IEEE Microwave Theory and Techniques Society (IEEE MTT-S) Microwave Prize (best Paper Award of the IEEE TRANSACTIONS ON MICROWAVE THEORY AND TECHNIQUES), the 1999 IEE Marconi Premium (best Paper Award of the *IEE Proceedings on Microwaves, Antennas and Propagation*), the 1999 URSI Young Scientist Award, the 2005 University of Massachusetts Dartmouth Scholar of the Year Award, the 2004 University of Massachusetts Dartmouth College of Engineering Dean's Recognition Award, the 1992 Belgrade Chamber of Industry and Commerce Best M.S. Thesis Award, the 2009, 2010, and 2011 Colorado State University Electrical and Computer Engineering Excellence in Teaching Award, the 2010 Colorado State University College of Engineering George T. Abell Outstanding Teaching and Service Faculty Award, and the 2012 Colorado State University System Board of Governors Excellence in Undergraduate Teaching Award.